

A Comparison Study on Coupling Effects in Balance Control Methods of Humanoid Robots through an Extended Task Space Formulation

Seungjae Yoo¹ ^a, Joonhee Jo^{1,2} ^b and Yonghwan Oh¹ ^c

¹*Korea Institute of Science and Technology, 5, Hwarang-ro 14-gil, Seongbuk-gu, Seoul, Republic of Korea*

²*University of Science and Technology, 217 Gajeong-ro Yuseong-gu, Daejeon, 34113, Republic of Korea*

Keywords: Humanoid, Whole-body Control, Balance, Extended Task Space, Null Space.

Abstract: Even though several control methods on the task space dynamics of humanoids have been proposed, they cannot cover the entire dynamics of the system since there are hidden null space dynamics due to kinematic redundancy. Besides, there are few studies on the coupling effects between task space and null space dynamics. Through an extended task space formulation, the coupling effects between each space are manifested because this form allows representing the entire system dynamics. Moreover, by using an adequate selection of weighting matrices, the coupling effects can be inertially decoupled. Regarding the effectiveness of the decoupling process, two whole-body control approaches and provide their mathematical comparisons is proposed. A kinematically decomposed control approach without the decoupling process is first introduced, and its extension to an inertially decoupled control approach is then developed. Furthermore, conventional operational space-based control is discussed to compare the above control approaches. This paper constructs a mathematical analysis of their relationships. Finally, simulation results are given in this paper to demonstrate the validity of the mathematical analysis.

1 INTRODUCTION


The consideration of robot dynamics is known to be important for higher control performance. For the manipulators, the control of end-effector, combined with interaction tasks, has been widely studied such as the computed torque (Kim et al., 2018b) (Kim et al., 2018a) and the impedance method (Ott et al., 2008). Moreover, the hidden null space dynamics was also analyzed for the kinematically redundant manipulator system (Oh et al., 1997), (Oh and Chung, 1999). The controller including the null space dynamics was shown to have a relatively robust property (Oh et al., 1998).


For humanoid robots, dynamics is also known to be important for the balance control because its base is not physically fixed to the world. That is widely considered as an underactuated and kinematically redundant system since the joints exist in spine. A lot of balance control methods (Koolen et al., 2016), (Herzog et al., 2016) have been proposed with re-


solving the null space motion due to its redundancy. For instance, the inverse kinematics (Nakanishi et al., 2007), (Mistry et al., 2008), the quadratic programming (Stephens and Atkeson, 2010), (Ott et al., 2011), the operational space (Sentis and Park, 2004), (Sentis and Khatib, 2005) and the passivity framework (Henze et al., 2016), (Hyon et al., 2007) had been addressed so far.

Even though the task space formulation can make the dynamic behavior of the humanoid robot, it is not sufficient to describe the entire behavior such as the null space motion. There is hidden null space dynamics and its effect has not been considered concretely in the robotics society. Through an extended task space formulation by parameterizing the minimal null space motion, an extended space dynamics is set up. Based on the formulation, it manifests the coupling effect between the task space and the null space and can be inertially decoupled between each space by the careful choice of weighting matrices.

In this paper, we present two extended task space control methods mainly and one task space control for the humanoid robot based on the computed torque method: kinematically decomposed control, inertially decoupled control and conventional task space con-

^a  <https://orcid.org/0000-0002-3367-3418>

^b  <https://orcid.org/0000-0002-6133-0754>

^c  <https://orcid.org/0000-0002-1109-305X>

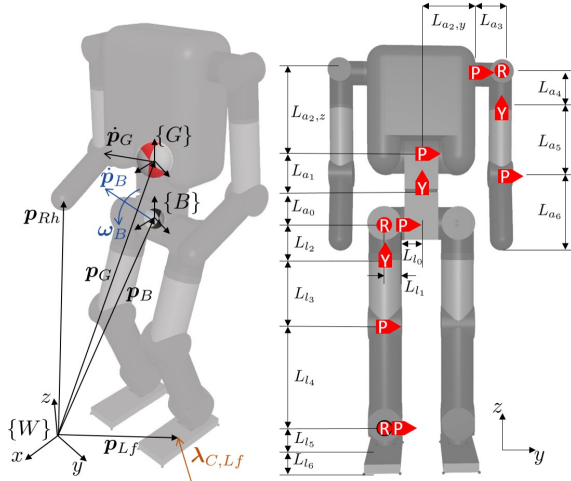


Figure 1: The humanoid model view: $\{W\}$ notes an world frame, $\{B\}$ notes a body frame, $\{G\}$ notes a frame at the center of mass.

control. The difference between methods is investigated in the situation where unexpected external force enters the system. It is worth to remark that the residual between desired and unexpected external force does not disturb the null space motion analytically due to the characteristic of the inertially decoupled case. In addition, the simulation result demonstrates the analysis of each characteristic.

The paper organized as follows. Section 2 describes the formulation of dynamics with regard to the extended task space from the joint space with the floating states. Section 3 describes the three control methods with the analysis of their characteristics and differences. Section 4 presents the proper reference planning and simulation results. Discussions of the result are also illustrated with some graphs and figures.

2 DYNAMICS FORMULATION FOR HUMANOID

The position of the center of mass (CoM) is important since it implies the overall momentum and acceleration of the system. Moreover, its characteristic can ease the complexity of deriving the dynamic formulation of the humanoid robot (Hyon et al., 2007). Therefore, the proposed generalized coordinates ξ is

$$\xi = \begin{pmatrix} v_G \\ \dot{q} \end{pmatrix} \in \mathbb{R}^{n+6}, \quad v_G = \begin{pmatrix} \dot{p}_G \\ \omega_B \end{pmatrix} \in \mathbb{R}^6$$

where $\dot{p}_G, \omega_B \in \mathbb{R}^3$ and $\dot{q} \in \mathbb{R}^n$ are linear velocity of CoM, angular velocity of the body and joint velocities as shown in figure 1, respectively.

The equation of motion with regard to ξ generally forms

$$\underbrace{\begin{bmatrix} M_{11} & M_{12} \\ M_{21} & M_{22} \end{bmatrix}}_M \underbrace{\begin{pmatrix} \dot{v}_G \\ \dot{q} \end{pmatrix}}_{\xi} + C\xi + \begin{pmatrix} \bar{m}\bar{g} \\ \mathbf{0} \end{pmatrix} = \xi_{\tau}^T \tau + J_C^T \lambda_C \quad (1)$$

where $M, C \in \mathbb{R}^{(n+6) \times (n+6)}$ are the inertia, Coriolis & Centrifugal matrices, \bar{m} is the total mass, $\bar{g} \in \mathbb{R}^6$ is the gravity vector, $\xi_{\tau} = [\mathbf{0}_6 \ E_n] \in \mathbb{R}^{n \times (n+6)}$ is the selection matrix, $\tau \in \mathbb{R}^n$ is the joint input torque, $J_C \in \mathbb{R}^{k \times (n+6)}$ is the constraint Jacobian, and $\lambda_C \in \mathbb{R}^k$ is the ground reaction force, respectively.

2.1 Task Space Dynamics of Humanoid Robots

Regarding control using the dynamics represented by used quantities such as end-effectors in Cartesian space, the task space coordinates is required. It can be obtained by the proposed transformation (Henze et al., 2016) as

$$\dot{x} = T\xi, \quad T = \begin{bmatrix} E_6 & \mathbf{0} \\ Q_T^T & \hat{J}_T \end{bmatrix} \in \mathbb{R}^{(m+6) \times (n+6)} \quad (2)$$

where $\dot{x} = (v_G \ \dot{x}_T) \in \mathbb{R}^{m+6}$ is the task space coordinates, $\dot{x}_T \in \mathbb{R}^m$ is the vector of end-effector velocities, and T is the transformation map, respectively. Q and \hat{J} denote the part of Jacobian where the former is related to v_G and the latter is related to \dot{q} as

$$\dot{x}_T = Q_T^T v_G + \hat{J}_T \dot{q}$$

where $Q_T \in \mathbb{R}^{6 \times m}$ and $\hat{J}_T \in \mathbb{R}^{m \times n}$. The general inverse of the transformation map is

$$T^{\#} = \begin{bmatrix} E_6 & \mathbf{0} \\ -\hat{J}_T^{\#} Q_T^T & \hat{J}_T^{\#} \end{bmatrix} \quad (3)$$

where $\hat{J}_T^{\#} \triangleq W_T^{-1} \hat{J}_T^T (\hat{J}_T W_T^{-1} \hat{J}_T^T)^{-1}$ is the generalized inverse of \hat{J}_T with the proper weight matrix $W_T \in \mathbb{R}^{n \times n}$.

By substituting (2) into (1), the equation of motion for the operational space is derived as

$$\Lambda \ddot{x} + \Gamma \dot{x} + \begin{pmatrix} \bar{m}\bar{g} \\ \mathbf{0} \end{pmatrix} = \begin{bmatrix} -Q_T \hat{J}_T^{\#T} \\ \hat{J}_T^{\#T} \end{bmatrix} \tau + \begin{pmatrix} \mathbf{0} \\ \tilde{\lambda}_C \end{pmatrix} \quad (4)$$

with $\Lambda = T^{\#T} M T^{\#}$, $\Gamma = T^{\#T} (C - M T^{\#T} \dot{T}) T^{\#} \in \mathbb{R}^{(m+6) \times (m+6)}$, $\tilde{\lambda}_C = \xi_C \lambda_C \in \mathbb{R}^m$, $\xi_C \in \mathbb{R}^{m \times k}$.

2.2 Dynamic Equations based on as Extended Task Space Formulation

The task space dynamics is not sufficient to describe the entire behavior of the robot since it has a lower

dimension than the joint space coordinates due to redundancy. Therefore, the consideration of the null space motion is required to figure out the overall motion of the robot. The extended task space formulation can visualize the hidden null space dynamics by parameterizing the minimal null space motion.

The definition of minimal null space motion $\dot{x}_N \in \mathbb{R}^r$ is proposed (Oh et al., 1997) (Oh and Chung, 1999) as follows

$$\dot{x}_N \triangleq \underbrace{(V^T W_N V)^{-1} V^T W_N \xi}_{J_N} = [Q_N^T \quad \hat{J}_N] \xi \quad (5)$$

with the general solution of (2)

$$\xi = T^\# \dot{x} + (E_{n+6} - T^\# T) \xi = T^\# \dot{x} + V \dot{x}_N \quad (6)$$

where $J_N \in \mathbb{R}^{r \times (n+6)}$ and $V = [0 \quad \hat{V}^T]^T \in \mathbb{R}^{(n+6) \times r}$ denote the Jacobian and the basis matrix of minimal null space, $Q_N \in \mathbb{R}^{6 \times r}$, $\hat{J}_N \in \mathbb{R}^{r \times n}$, $r = n - m$ with the proper weighting matrix $W_N \in \mathbb{R}^{(n+6) \times (n+6)}$, respectively.

The extended task space $\dot{x}_E = (v_G \quad \dot{x}_T \quad \dot{x}_N) \in \mathbb{R}^{n+6}$ is defined as follows.

$$\dot{x}_E = T_E \xi, \quad T_E = \begin{bmatrix} E_6 & 0 \\ Q_N^T & \hat{J}_N \\ Q_N^T & \hat{J}_N \end{bmatrix} \in \mathbb{R}^{(n+6) \times (n+6)} \quad (7)$$

where T_E is the extended transformation map. The general inverse of this map is

$$T_E^{-1} = \begin{bmatrix} E_6 & 0 & 0 \\ -\hat{J}_N^{\#T} Q_N^T & -\hat{J}_N^{\#T} Q_N^T & \hat{J}_N^{\#T} \\ \hat{J}_N^{\#T} & \hat{J}_N^{\#T} & \hat{J}_N^{\#T} \end{bmatrix} \quad (8)$$

where $\hat{J}_N^{\#} = \hat{V} \in \mathbb{R}^{n \times r}$.

By substituting (7) into (1), the equation of motion for an extended task space is derived as

$$\Lambda_E \ddot{x}_E + \Gamma_E \dot{x}_E + \begin{pmatrix} \bar{m}\bar{g} \\ 0 \\ 0 \end{pmatrix} = \begin{bmatrix} -Q_T \hat{J}_T^{\#T} - Q_N \hat{J}_N^{\#T} \\ \hat{J}_T^{\#T} \\ \hat{J}_N^{\#T} \end{bmatrix} \tau + \begin{pmatrix} 0 \\ \tilde{\lambda}_C \\ 0 \end{pmatrix} \quad (9)$$

where $\Lambda_E = T_E^{-T} M T_E^{-1}$, $\Gamma_E = T_E^{-T} (C - M T_E^{-1} \dot{T}_E) T_E^{-1} \in \mathbb{R}^{(n+6) \times (n+6)}$. In addition, the relation between Λ_E , Γ_E and Λ , Γ can be visualized from the following equations.

$$\Lambda_E = \begin{bmatrix} \Lambda_G \\ \Lambda_T \\ \Lambda_N \end{bmatrix} = \begin{bmatrix} \tilde{\Lambda}_G & \Lambda_{GN} \\ \tilde{\Lambda}_T & \Lambda_{TN} \\ \tilde{\Lambda}_N & \Lambda_{NN} \end{bmatrix} = \begin{bmatrix} \Lambda & \tilde{\Lambda}_N^T \\ \tilde{\Lambda}_N & \Lambda_{NN} \end{bmatrix} \quad (10)$$

$$\Gamma_E = \begin{bmatrix} \Gamma_G \\ \Gamma_T \\ \Gamma_N \end{bmatrix} = \begin{bmatrix} \tilde{\Gamma}_G & \Gamma_{GN} \\ \tilde{\Gamma}_T & \Gamma_{TN} \\ \tilde{\Gamma}_N & \Gamma_{NN} \end{bmatrix} = \begin{bmatrix} \Gamma & \tilde{\Gamma}_N^T \\ \tilde{\Gamma}_N & \Gamma_{NN} \end{bmatrix} \quad (11)$$

where Λ_{NN} , Γ_{NN} , $\tilde{\Lambda}_N$, $\tilde{\Gamma}_N$ denote the hidden null space dynamics. As shown in (10) and (11), $\tilde{\Lambda}_N$, $\tilde{\Gamma}_N$ makes coupling effect between the task space and the null space motion because it is not zero. In this sense, the null space motion could interfere with the task space motion if there is not considerations on the coupling effect.

3 BALANCE CONTROLLER DERIVATION FOR HUMANOID

In this section, the controllers based on the computed torque method are developed through the proposed formulation with the quadratic programming.

The closed-loop behavior candidate based on the computed torque method is

$$\Lambda_E (\ddot{e}_E + K_{D,E} \dot{e}_E + K_{P,E} e_E) = \begin{pmatrix} 0 \\ \tilde{\lambda}_C^{opt} \\ 0 \end{pmatrix} - \begin{pmatrix} 0 \\ \tilde{\lambda}_C \\ 0 \end{pmatrix} \quad (12)$$

where $e_E = x_{E,d} - x_E$ is the error of the extended tasks. To achieve (12), the input joint torque forms as follows.

$$\tau = \begin{bmatrix} \hat{J}_T \\ \hat{J}_N \end{bmatrix}^T \left(\begin{bmatrix} \Lambda_T \\ \Lambda_N \end{bmatrix} \ddot{x}_E^{ref} + \begin{bmatrix} \Gamma_T \\ \Gamma_N \end{bmatrix} \dot{x}_E - \begin{pmatrix} \tilde{\lambda}_C^{opt} \\ 0 \end{pmatrix} \right) \quad (13)$$

with

$$\ddot{x}_E^{ref} \triangleq \ddot{x}_{E,d} + K_{D,E} \dot{e}_E + K_{P,E} e_E \quad (14)$$

$$\tilde{\lambda}_C^{opt} = \operatorname{argmin} \left(\delta_G^T W_G \delta_G + \tilde{\lambda}_C^{optT} W_C \tilde{\lambda}_C^{opt} \right) \quad (15)$$

and

$$\delta_G \triangleq \bar{\Lambda}_E \ddot{x}_E^{ref} + \bar{\Gamma}_E \dot{x}_E + \bar{m}\bar{g} - Q_T \tilde{\lambda}_C^{opt}$$

$$\bar{\Lambda}_E = \Lambda_G + Q_T \Lambda_T + Q_N \Lambda_N$$

$$\bar{\Gamma}_E = \Gamma_G + Q_T \Gamma_T + Q_N \Gamma_N$$

where $K_{P,E}$ and $K_{D,E}$ denote the stiffness and damping matrices, W_G and W_C are positive definite weighting matrices, respectively. The quadratic programming in (15) is conducted based on the proper equality and inequality constraints as follows.

$$p_{CoP} \in A_{CoP}$$

$$f_{i,x} \leq \mu_x f_{i,z}$$

$$f_{i,y} \leq \mu_y f_{i,z}$$

The p_{CoP} and the A_{CoP} denote the position of center of pressure (CoP) and the area where it should be, and $f_i = (f_{i,x} \quad f_{i,y} \quad f_{i,z})$, $i = 1, \dots, 4$ is an external force for each foot as shown in figure 2.

For the ideal case, with the assumptions that $\delta_C \triangleq \tilde{\lambda}_C^{opt} - \tilde{\lambda}_C \rightarrow 0$ and $\delta_G \rightarrow 0$, the (12) shows exponentially convergence property since

$$\ddot{e}_E + K_{D,E} \dot{e}_E + K_{P,E} e_E = 0. \quad (16)$$

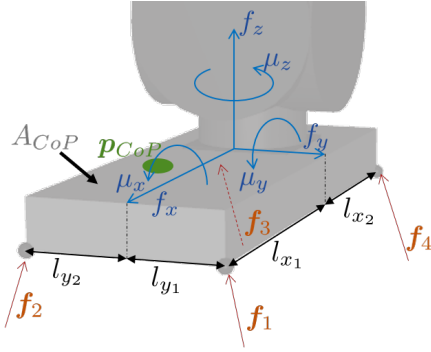


Figure 2: The linear and angular force at each foot based on the ground reaction forces from 4 point contacts.

3.1 Comparison between Kinematically Decomposed Control and Inertially Decoupled Control

It is called the kinematically decomposed control (KDC) for the case that $\mathbf{W}_T, \mathbf{W}_N$ are identity matrices. Then, there are coupling effect as shown in the following original closed-loop behavior

$$\begin{bmatrix} \Lambda & \tilde{\Lambda}_N^T \\ \tilde{\Lambda}_N & \Lambda_{NN} \end{bmatrix} \begin{pmatrix} \ddot{e} + \mathbf{K}_D \dot{e} + \mathbf{K}_P e \\ \ddot{e}_N + \mathbf{K}_{D,N} \dot{e}_N + \mathbf{K}_{I,N} \int \dot{e}_N dt \end{pmatrix} = \begin{pmatrix} \delta \\ \mathbf{0} \end{pmatrix} \quad (17)$$

where $\dot{e} = \dot{x}_d - \dot{x}$, $\dot{e}_N = \dot{x}_{N,d} - \dot{x}_N$ denote the part of error \dot{e}_E and $\mathbf{K}_P, \mathbf{K}_D, \mathbf{K}_{D,N}, \mathbf{K}_{I,N}$ are proper gains corresponding with $\mathbf{K}_{P,E}, \mathbf{K}_{D,E}$, respectively. The residual $\delta \triangleq (\delta_G \ \delta_C) \in \mathbb{R}^{m+6}$ is not generally zero since the ground reaction force $\tilde{\lambda}_C$ is the external environmental parameter. For instance, the impulsive force could occur when a foot lands or collides with an object. It is quite difficult to obtain the precise $\tilde{\lambda}_C^{opt}$ satisfying $\delta_C = \mathbf{0}$ at an instance. Therefore, due to the coupling effect, the residual could impede conservation on the null space motion and subsequent unstable null space dynamics could affect the task space motion.

On the other hand, the inertia matrix (10) can be decoupled between the task space and the null space since $\tilde{\Lambda}_N = \mathbf{0}$ by selecting proper weighting matrices $\mathbf{W}_T = \mathbf{M}_{22}$ and $\mathbf{W}_N = \mathbf{M}$. It is called the inertially decoupled control (IDC) and its closed-loop behavior forms as following

$$\Lambda(\ddot{e} + \mathbf{K}_D \dot{e} + \mathbf{K}_P e) = \delta \quad (18)$$

$$\ddot{e}_N + \mathbf{K}_{D,N} \dot{e}_N + \mathbf{K}_{I,N} \int \dot{e}_N dt = \mathbf{0} \quad (19)$$

As shown in (18) and (19), the closed-loop system of null space is completely decoupled with the task space and the δ only affect to the task space motion. It is worthwhile that the null space motion does not

affect the task space completely on the inertially decoupled controller.

3.2 Reformulation of Conventional Operational Space based Control in Terms of Inertially Decoupled Control

The operational space dynamics (4) derives the joint input torque similar with (13) as follows.

$$\tau = \hat{J}_T^T (\tilde{\Lambda}_T \ddot{x}^{ref} + \tilde{\Gamma}_T \dot{x} - \tilde{\lambda}_C^{opt}) + \mathbf{P}_N^T \tau_q \quad (20)$$

with

$$\ddot{x}^{ref} \triangleq \ddot{x}_d + \mathbf{K}_D \dot{e} + \mathbf{K}_P e \quad (21)$$

$$\tau_q = \mathbf{K}_N (q_d - q) - \mathbf{D}_N \dot{q} \quad (22)$$

where

$$\delta_G \triangleq \tilde{\Lambda} \ddot{x}^{ref} + \tilde{\Gamma} \dot{x} + \tilde{m} \tilde{g} - \mathbf{Q}_T \tilde{\lambda}_C$$

$$\tilde{\Lambda} = \tilde{\Lambda}_G + \mathbf{Q}_T \tilde{\Lambda}_T$$

$$\tilde{\Gamma} = \tilde{\Gamma}_G + \mathbf{Q}_T \tilde{\Gamma}_T$$

where $\mathbf{P}_N = \mathbf{E}_n - \hat{J}_T^\# \hat{J}_T$ is the null projection matrix with $\mathbf{W}_T = \mathbf{M}_{22}$. It is called the operational space control (OSC) since it focuses on the task space with the conventional null space control by $\mathbf{P}_N^T \tau_q$. According to (6) and (8),

$$\mathbf{P}_N = \hat{V} \hat{J}_N \quad (23)$$

since $\mathbf{T}_E^{-1} \mathbf{T}_E = \mathbf{T}^\# \mathbf{T} + \mathbf{V} \mathbf{J}_N = \mathbf{E}_{n+6}$. By substituting τ as an input into (9), the closed loop behavior is derived as follows.

$$\Lambda(\ddot{e} + \mathbf{K}_D \dot{e} + \mathbf{K}_P e) = \delta - \tilde{\Gamma}_N^T \dot{x}_N \quad (24)$$

$$\Lambda_{NN} \ddot{x}_N + \Gamma_{NN} \dot{x}_N + \tilde{\Gamma}_N \dot{x} = \hat{V}^T \tau_q \quad (25)$$

Although it is already inertially decoupled since $\tilde{\Lambda}_N = \mathbf{0}$ with assumption $\delta \rightarrow \mathbf{0}$, the coupling effect $\tilde{\Gamma}_N^T \dot{x}_N$ enters to the task space dynamics as (24). The torque for null motion can be expressed with regard to the desired null space motion defined as following

$$\dot{x}_{N,d} \triangleq \mathbf{J}_N \mathbf{M}^{-1} \nabla U(q) \quad (26)$$

with the potential $U(q) = \sum_i \frac{1}{2} \eta_i (q_{i,d} - q_i)$. In addition, $\mathbf{K}_N = \kappa \mathbf{E}_n$, $\mathbf{K}_{N,D} = \kappa \mathbf{E}_r$ and $\mathbf{K}_D = \kappa \mathbf{M}_{22}$ with the scalar gain κ as (Oh et al., 1998). The equivalent null space torque with respect to (13) is

$$\mathbf{P}_N^T \tau_q = \kappa \hat{J}_N^T \Lambda_{NN} \dot{e}_N \quad (27)$$

Therefore, it gives the same effect at setting $\dot{x}_{N,d} = \mathbf{0}$, $\mathbf{K}_{I,N} = \mathbf{0}$ and excluding the compensating term $\tilde{\Gamma}_N \dot{x}$. In other words, the above equation shows that the control input through (27) has some limitation for the precise tracking performance on the null space. In this sense, it is expected that the error \dot{e}_N would not show convergence with the input (20) since the closed-loop behavior on the null space (25) cannot be expressed as an error dynamics form.

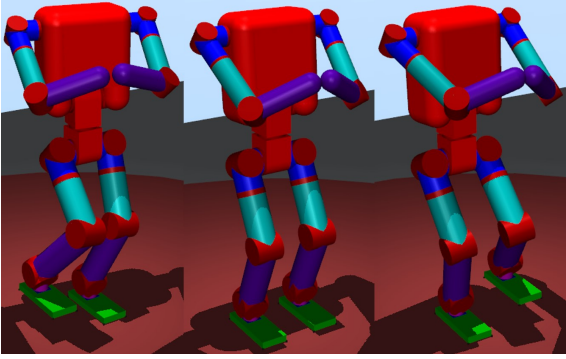


Figure 3: Simulation model (MuJoCo).

Table 1: Simulation Model Parameters.

Parameter	Length(m)	Mass(kg)	Inertia($10^{-4}kg \cdot m$)
L_{l_0}	0.05	5	diag(135.0, 135.0, 83.00)
L_{a_0}	0.1		
L_{l_1}	0.06	0.5	diag(4.625, 6.250, 4.625)
L_{l_2}	0.1	0.5	diag(7.292, 7.292, 6.250)
L_{l_3}	0.2	1.5	diag(59.00, 19.00, 59.00)
L_{l_4}	0.3	1.5	diag(19.00, 122.0, 122.0)
L_{l_5}	0.07	0.25	diag(3.125, 2.583, 2.583)
L_{l_6}	0.03	0.75	diag(45.00, 6.813, 40.00)
L_{a_1}	0.1	5	diag(83.00, 83.00, 83.00)
$L_{a_2,z}$	0.25	15	diag(1450., 2405., 1250.)
$L_{a_2,y}$	0.16		
L_{a_3}	0.08	0.5	diag(3.792, 2.250, 3.792)
L_{a_4}	0.1	0.5	diag(5.292, 5.292, 2.250)
L_{a_5}	0.2	1.0	diag(36.00, 4.500, 36.00)
L_{a_6}	0.2	1.0	diag(4.500, 36.00, 36.00)

4 EVALUATION OF SIMULATION RESULTS

The simulation was developed with the proposed controller based on the humanoid model as shown in figure 3. Its specific parameters are depicted in figure 1 and Table 1 such as a mass, inertia and length of each link. Its height and total mass are designed to be $1.2m$ and $41kg$. It has 28 degrees of freedom (DoF) with 22 joints in which each leg has 6 and each arm has 4 and a spine has 2 joints. Each dimension of the space is

$$n = 22, m = 18, r = 4, k = \begin{cases} 6 & \text{(Single support)} \\ 12 & \text{(Double support)} \end{cases}$$

The position, orientation, linear and angular velocities at the body frame ($p_B, R_B, \dot{p}_B, \omega_B$) are considered as known values by the suitable IMU sensor and the estimator. The simulation was performed by use of a commercial software MuJoCo (Todorov et al., 2012) with Win 32 compiler.

Because the extended task space formulation (9) requires heavy computation due (Prete et al., 2015) to M^{-1} , $\frac{d}{dt}(M^{-1})$ and $M_{12} \neq 0$, it needs a substantial time interval for real-time control. However, the fol-

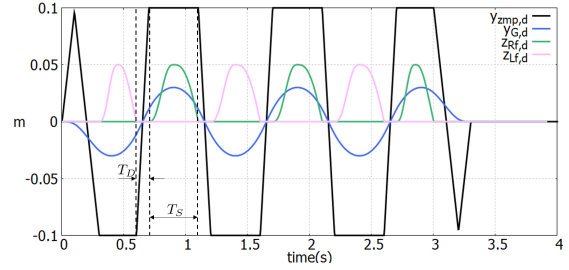


Figure 4: ZMP/CoM trajectory of frontal plane. The $z_{Lf,d}$ and $z_{Rf,d}$ denotes the desired z directional motion of each foot for marching in place. $T_S = 0.1s$ and $T_D = 0.4s$ are time intervals for single and double supported cases, respectively.

lowing input form is exactly equivalent with (13) and demands relatively light computation.

$$\tau = \xi_{\tau}^T \left(M \xi^{ref} + C \xi - T_E^T \begin{pmatrix} 0 \\ \tilde{\lambda}^{opt} \\ 0 \end{pmatrix} \right) \quad (28)$$

with

$$\xi^{ref} = T_E^{-1} (\ddot{x}_E^{ref} - \dot{T}_E \xi) \quad (29)$$

With the input form (28), the simulation is conducted with 1Khz of solving rate and 500hz of control rate.

4.1 Reference Planning for the Motion of Marching in Place

To figure out the effect of δ_C , the task space reference is designed for marching in place. The motion for center of mass on the frontal plane is obtained by solving the equation of inverted pendulum as follows.

$$\ddot{p}_{G,y} = \omega^2 (p_{G,y} - y_{zmp}), \quad \omega^2 = \frac{g}{h_z} \quad (30)$$

where h_z is height of CoM from the ground, $g = 9.81m/s^2$ is the gravity acceleration and y_{zmp} denotes zero moment point (ZMP), respectively. According to the above differential equation, the reference ZMP and CoM trajectories in figure 4 is achieved (Oh et al., 2006).

Each foot is raised up and down in the single support duration while the other end-effector and CoM motions are fixed with regard to the world frame.

The desired null space motion $\dot{x}_{N,d}$ is designed as (26) where $q_{i,d} = 0$ and $\eta_i = 0$ for all i except $\eta_{13} = \eta_{14} = \eta_{16} = \eta_{20} = 1$.

4.2 Evaluation of the Results

In this section, it shows the task space performance and the null space motion through the simulation results. To exaggerate the coupling effect due to the

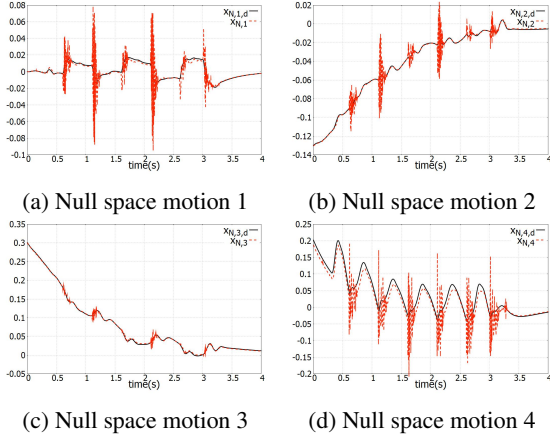


Figure 5: Null space motion on the kinematically decomposed control. Blue and red lines denote the desired and the present null space motion, respectively.

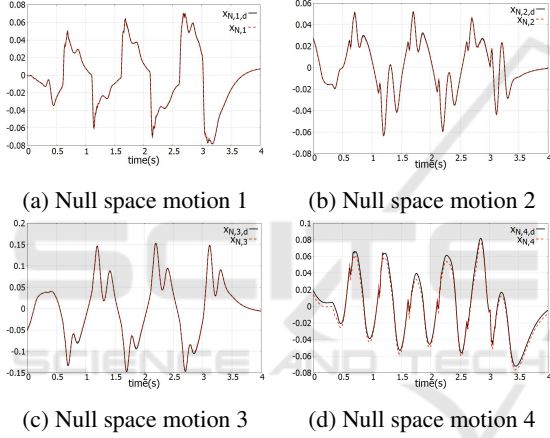


Figure 6: Null space motion on the inertially decoupled control. Blue and red lines denote the desired and the present null space motion, respectively.

residual δ_C , each foot collides with the ground at $-0.5m/s$ during the marching motion as shown in figure 3 and figure 4. Because the $\tilde{\lambda}_C^{opt}$ in (15) is handled as feedforward, the residual exists generally and it would be especially emphasized at colliding with other objects such as the ground in landing motion.

Figure 5 and figure 6 present the null space motion of the KDC and IDC, respectively. The null space tasks \dot{x}_N does not have any units since it is independent with the Cartesian space tasks and does not have physical meaning. In KDC, the force residual δ_C affect the null space motion as its closed loop behavior (17), which is shown in figure 5.

In contrast, the IDC method does not transfer its effect to the null space motion analytically as the closed loop behavior (18) and (19). The simulation result demonstrates that the motion of null space tasks

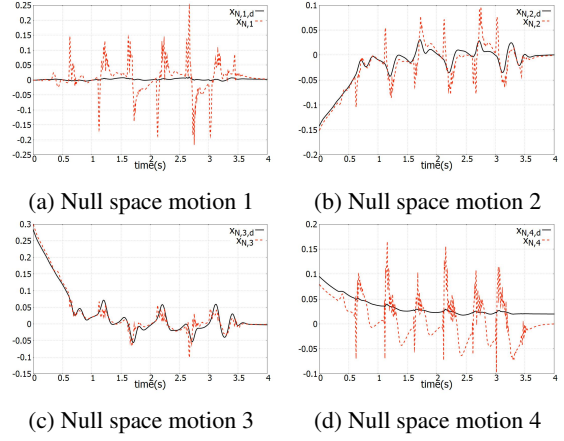


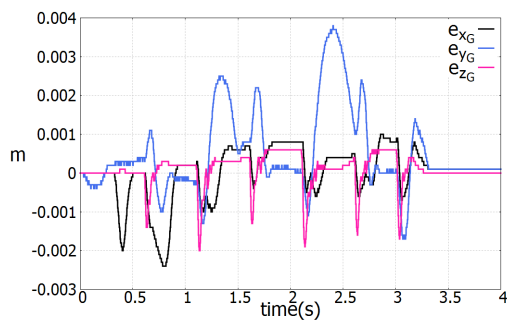
Figure 7: Null space motion on the operational space control. Blue and red lines denote the desired and the present null space motion, respectively.

is almost unaffected by the residual δ_C with respect to the kinematically decomposed case at landing each foot.

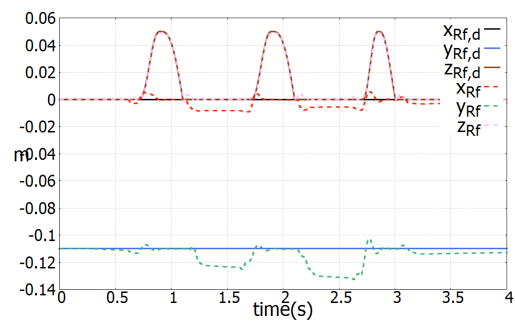
The figure 7 shows the null space motion on OSC. Because it does not contain the desired acceleration, integrator and compensator for the null space as (27), it is expected that there is some limitation for the tracking performance. The simulation result presents that the null space motion does not show damping response and convergence of the steady error. In addition, even though it is also one of the inertially decoupled cases due to $\tilde{\Lambda}_N = 0$, the larger effect of the residual δ_C is shown compared to figure 6. It could be explained because it does not compensate for the coupling effect $\tilde{\Gamma}_N \dot{x}$.

Figure 8 shows the position error of CoM and it describes the tracking performance on the task space with the given reference. The CoM motions followed well for all controllers, but the magnitude of the error is smallest for IDC and largest for OSC. It gives an example that the task space motion is, although small, impeded by the inertially coupling effect through $\tilde{\Lambda}_N$ on KDC and the uncompensated dynamic coupling effect $\tilde{\Gamma}_N^T \dot{x}_N$ on OSC. Therefore, there is a possibility that the more vigorous motion there is in the null space, the more coupling effect that disturbs the task space motion at using KDC or OSC.

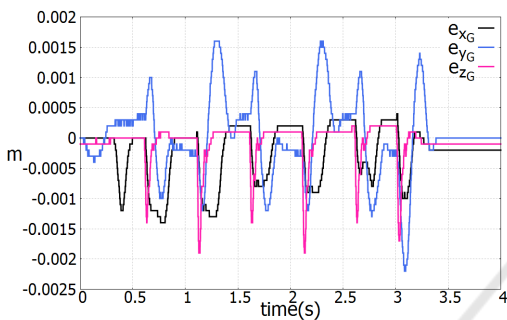
Most interesting results in this simulation are suggested by the motion of each foot figure 9. With regard to the marching motion, each foot does not have x and y directional motion, albeit it moves up and down to the z -axis. Therefore, the existence of error when the z -axis reference is zero indicates an example of a slip for each foot. A comparison of figure 9a, figure 9b and figure 9c shows that the smallest slip appears in the IDC. It suggests that the inertially cou-



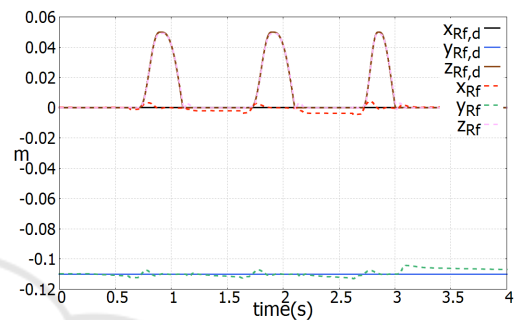
(a) The error of CoM on KDC



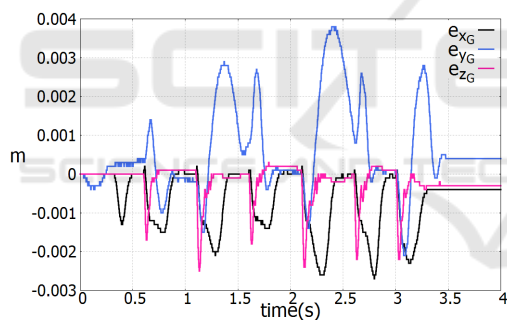
(a) The motion of the right foot on KDC



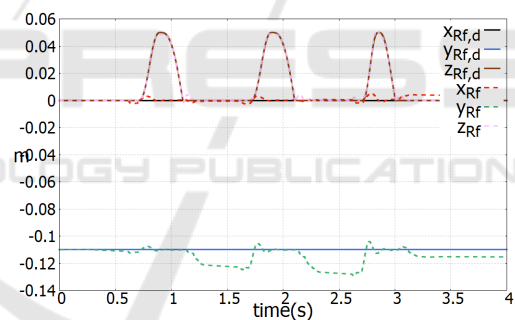
(b) The error of CoM on IDC



(b) The motion of the right foot on IDC



(c) The error of CoM on OSC



(c) The motion of the right foot on OSC

Figure 8: Errors of the CoM on the each controller.

Figure 9: Motion of the right foot on the each controller.

pling effect at KDC and the uncompensated coupling effect at OSC have an influence on the landing situation, and the inertially decoupling process of IDC has a positive effect for such a situation.

5 CONCLUSION

In this paper, it present three whole-body controllers for the balance of humanoids by using an extended task space formulation. The dynamic coupling effects are manifested since the extended task space form can represent the entire system dynamics. Through the decoupling process by selecting the weighting matrices carefully, the effects are inertially decoupled be-

tween each space. On the comparison study, we compare cases of the controller with or without the decoupling process mathematically to confirm the impact of coupling effects. Moreover, the conventional operational space based control is also analyzed in the absence of any compensator for showing the convergence of the errors in the closed-loop behavior.

The simulation model has 28 degrees of freedom with 22 joints. The robot conducts marching motion to generate the unexpected ground reaction force while the other position of CoM and end-effectors are fixed. The simulation result shows the coupling effect between task space and null space. The inertially decoupled control method reduces its effect conspicuously. In addition, the simulation results back up the

analysis that tracking performance of the null space motion would not be precise on the conventional operational space based control due to the lacking in compensator. Therefore, while it is the simplest conventional one, the results indicate the importance of consideration for the null space dynamics.

REFERENCES

- Henze, B., Roa, M. A., and Ott, C. (2016). Passivity-based whole-body balancing for torque-controlled humanoid robots in multi-contact scenarios. *Intl. Journal of Robotics Research*.
- Herzog, A., Rotella, N., Mason, S., Grimminger, F., Schaal, S., and Righetti, L. (2016). Momentum control with hierarchical inverse dynamics on a torque-controlled humanoid. *Autonomous Robots*.
- Hyon, S.-H., Hale, J. G., and Cheng, G. (2007). Full-body compliant human-humanoid interaction: Balancing in the presence of unknown external forces. *IEEE Transactions on Robotics*.
- Kim, J. H., moon Hur, S., and Oh, Y. (2018a). l_1 robustness of computed torque method for robot manipulators. *IEEE Intl. Conf. on Robotics and Automation*.
- Kim, J. H., moon Hur, S., and Oh, Y. (2018b). A study on the l_∞/l_2 performance of a computed torque controller. *IEEE Intl. Conf. on Industrial Technology*.
- Koolen, T., Bertrand, S., Thomas, G., De Boer, T., Wu, T., Smith, J., Engelsberger, J., and Pratt, J. (2016). Design of a momentum-based control framework and application to the humanoid robot atlas. *International Journal of Humanoid Robotics*.
- Mistry, M., Nakanishi, J., Cheng, G., and Schaal, S. (2008). Inverse kinematics with floating base and constraints for full body humanoid robot control. *IEEE-RAS Intl. Conf. on Humanoid Robots*.
- Nakanishi, J., Mistry, M., and Schaal, S. (2007). Inverse dynamics control with floating base and constraints. *IEEE Intl. Conf. on Robotics and Automation*.
- Oh, Y. and Chung, W.-K. (1999). Disturbance-observer-based motion control of redundant manipulators using inertially decoupled dynamics. *IEEE/ASME Transaction on Mechatronics*.
- Oh, Y., Chung, W.-K., and Youm, Y. (1997). Extended impedance control of redundant manipulators using joint space decomposition. *IEEE Intl. Conf. on Robotics and Automation*.
- Oh, Y., Chung, W.-K., and Youm, Y. (1998). Extended impedance control of redundant manipulators based on weighted decomposition of joint space. *Journal of Robotic Systems*.
- Oh, Y., ho Ahn, K., Kim, D., and Kim, C. (2006). An analytical method to generate walking pattern of humanoid robot. *Annual Conference of the IEEE Industrial Electronics Society*.
- Ott, C., Albu-Schaffer, A., Kugi, A., and Hirzinger, G. (2008). On the passivity-based impedance control of flexible joint robots. *IEEE Transactions on Robotics*.
- Ott, C., Roa, M. A., and Hirzinger, G. (2011). Posture and balance control for biped robots based on contact force optimization. *IEEE-RAS Intl. Conf. on Humanoid Robots*.
- Prete, A. D., Nori, F., Metta, G., and Natale, L. (2015). Prioritized motion-force control of constrained fully-actuated robots: "task space inverse dynamics". *Robotics and Autonomous Systems*.
- Sentis, L. and Khatib, O. (2005). Control of free-floating humanoid robots through task prioritization. *IEEE Intl. Conf. on Robotics and Automation*.
- Sentis, L. and Park, J. (2004). Whole-body dynamic behavior and control of human-like robots. *Intl. Journal of Humanoid Robotics*.
- Stephens, B. J. and Atkeson, C. G. (2010). Dynamic balance force control for compliant humanoid robots. *IEEE/RSJ Intl. Conf. on Intelligent Robots and Systems*.
- Todorov, E., Erez, T., and Tassa, Y. (2012). Mujoco: A physics engine for model-based control. *IEEE Intl. Conf. on Robotics and Systems*.